Mechanism of Elastic Softening Behavior in a Superlattice

Nobutomo Nakamura,* Hirotsugu Ogi, Takeshi Yasui, Makoto Fujii, and Masahiko Hirao

Graduate School of Engineering Science, Osaka University, Machikaneyama 1-3, Toyonaka, Osaka 560-8531, Japan

(Received 10 January 2007; published 19 July 2007)

We measured the out-of-plane elastic constants C_{33} of a Co/Pt superlattice by picosecond ultrasound, and found that they were closely related to the thickness ratio of Co and Pt layers; C_{33} was smaller than the prediction from the bulk values except for a specific thickness ratio. This behavior can be explained by the weak bonding at the interfaces that occurs to reduce the elastic strain energy, not by the interfacial strain. This view explained the relationship among C_{33}, the elastic strain energy, and perpendicular magnetic anisotropy.

DOI: 10.1103/PhysRevLett.99.035502 PACS numbers: 62.25.+g, 43.58.+z, 75.50.Ss

The superlattice has been attracting a lot of attention because of its anomalous properties. Among them, its property of elasticity has been investigated since the report of the supermodulus effect [1]. Although many researchers reached negative results from experiments [2–6] and atomistic-based simulations [7,8], it is still an open question. Among the independent elastic constants, C_{ij}, the out-of-plane elastic constant C_{33} showed a common behavior in several superlattice systems: as the bilayer thickness Λ decreased, C_{33} drastically decreased [9,10]. The previous studies concluded that C_{33} was closely related with the lowered interface stiffness due to the lattice misfit. However, there are other possible mechanisms such as the alloy phase and weak-bonding regions at the interfaces which have not been sufficiently discussed, and their contributions need to be reconsidered. This Letter aims to clarify the mechanism of the anomalous elastic behavior of superlattice and establish the comprehensive elastic model that can consistently explain the elastic property, as well as the magnetic property, of superlattice.

We studied Co/Pt superlattice for three reasons. First, it involves a large lattice misfit and high binding affinity between Co and Pt to make the coherent interfaces. The interatomic distance of Pt is larger than that of Co by 10.7%, and the lattice misfit introduces elastic strain larger than 0.05 in magnitude. This strain may be large enough to modify C_{ij} through the anharmonic interatomic potential. Second, the biaxial Poisson's ratio of Pt is large [11], indicating that the Pt film is easily deformed in the out-of-plane direction by the in-plane biaxial strain. The above two characteristics of Co/Pt superlattice are suitable for evaluating the contribution of the strain dependence of the modulus. Third, Co/Pt superlattice shows high perpendicular magnetic anisotropy (PMA), and the lattice coherency is easily evaluated by the degree of PMA. The easy magnetization direction of magnetic thin film is usually parallel to the film surface because of predominance of the shape-magnetic anisotropy [12]. However, in some superlattices, it is perpendicular to the film surface when the thickness of the magnetic material is of the order of angstrom, which is called PMA [13]. The Co/Pt superlattice is the well-known system showing strong PMA, for which large elastic strain at the interfaces is indispensable [14,15]. Therefore, the Co/Pt superlattice is an ideal system for clarifying the mechanism of the anomalous elasticity.

A series of Co/Pt superlattice thin films was deposited on (001) Si substrates by magnetron sputtering. A Pt-buffer layer of 16 Å was first deposited. In order to change the strain in Co and Pt layers, we varied the thickness ratio between Co and Pt. The Co-layer thickness of six specimens was fixed to be 4 Å, and the Pt-layer thickness was changed to be 2, 4, 8, 12, 16, and 20 Å. We deposited the films on several substrates simultaneously to confirm reproducibility. Two other specimens had a thickness ratio of d_{Co}:d_{Pt} = 1:4, and the bilayer thicknesses Λ ($= d_{Co} + d_{Pt}$) were 100 and 200 Å. The number of bilayers was changed to keep the total film thickness of 800 Å for all eight specimens. Bilayer thickness was determined by the x-ray total reflectivity measurement [16], and the total film thickness was determined from the bilayer thickness and the number of the bilayers. For all specimens, we observed sharp satellite peaks, which confirmed good periodicity.

The picosecond-laser ultrasound technique found by Thomsen *et al.* [17] enables one to determine the round-trip time of coherent acoustic phonons in GHz frequencies propagating in the film-thickness direction of a thin film. Film's C_{33} is determined from the round-trip time Δt, the mass density ρ, and the film thickness d, through $C_{33} = \rho(2d/\Delta t)^2$. We used the pulse-laser beam of 800 nm wavelength with 100-fs duration. It was separated into the pump and probe beams with power of 10 and 5 mW, respectively. Figure 1 shows the typical responses of the reflectivity variation detected by the probe beam; we observe five echoes of the longitudinal wave. After eliminating the background due to thermal phonons, we calculated the autocorrelation function with the first echo as the reference; the fifth echo is clearly visible. By this means, we yielded Δt within the error limit of 2%.

We evaluated PMA by measuring the effective magnetic anisotropy energy K_{eff} ($= U_{\parallel} - U_{\perp}$), where $U_{\parallel}$ is the

 © 2007 The American Physical Society

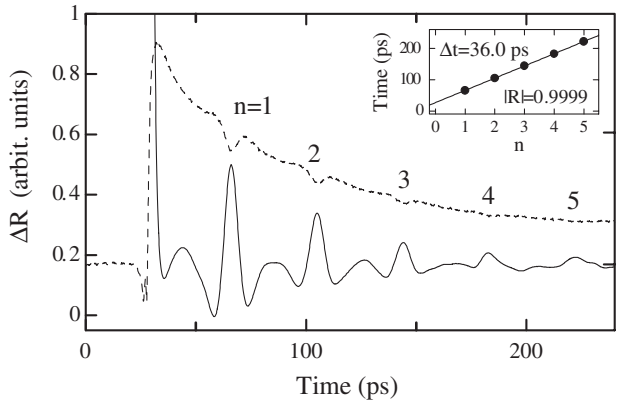

FIG. 1. Reflectivity change determined by the probe beam. As-measured multiple reflection echoes in Pt(16 Å)/[Co(4 Å)/Pt(8 Å)]$_{67}$ are denoted by the broken line, and the autocorrelation function of the observed data by the solid line. Δt is determined from the relationship between n and the individual transit times (see inset).

total energy of the system per unit volume of Co with the in-plane magnetization, and $U_\perp$ is that with the out-of-plane magnetization. When $U_\perp < U_\parallel$, $K_{\rm eff}$ becomes positive, and the superlattice shows PMA. $K_{\rm eff}$ is determined from the area surrounded by the initial-magnetization curves for the in-plane and out-of-plane directions [15]. Figure 2(a) shows the relationship between Λ and C_{33} of Co/Pt superlattice. C_{33} shows the maximum at $\Lambda = 12$ Å which has never been observed in any superlattice systems. Figure 2(b) shows the relationship between Λ and $K_{\rm eff}$. The vertical axis is normalized by the shape-magnetic-anisotropy energy K_s ($= NI_s^2/2\mu_0$) [12] (I_s: saturation magnetization; N: demagnetization factor of thin film ($N = 1$); μ_0: permeability of vacuum). $K_{\rm eff}$ shows large values for 12 Å $< \Lambda <$ 24 Å and PMA disappears when $\Lambda >$ 100 Å. Considering that a large strain is required to achieve high PMA, Co/Pt superlattice films of $\Lambda =$ 6–24 Å have grown epitaxially at the interfaces, but the other two thicker films barely grow epitaxially. Figure 3 plots the measured C_{33} normalized by the bulk value calculated for Co(hcp)/Pt superlattice using the rule of mixture, $C_{33}^{\rm bulk} = (f_{\rm Co}/C_{33}^{\rm Co} + f_{\rm Pt}/C_{33}^{\rm Pt})^{-1}$, where f_i is the volume fraction of the component i. For this, we used the reported C_{ij} of bulk hcp-Co [18] and Pt [19]. At room temperature, bulk Pt takes fcc structure, and (111) plane is the close-packed plane. In bulk Co, hcp is the stable structure at room temperature. However, in Co/Pt superlattice thin films, some reports suggest that fcc Co is stabilized when its thickness is less than 4 Å [20,21]. Close-packed planes of hcp and fcc Co are (0001) and (111) planes, respectively. In the following discussion, we therefore consider both hcp and fcc Co for Co layers.

We consider three mechanisms that can affect C_{33}. The first is the interfacial strain, which has been considered as the dominant factor for the softened superlattice. Clemens and Eesley [9] predicted the strain-dependent C_{33}^s by the

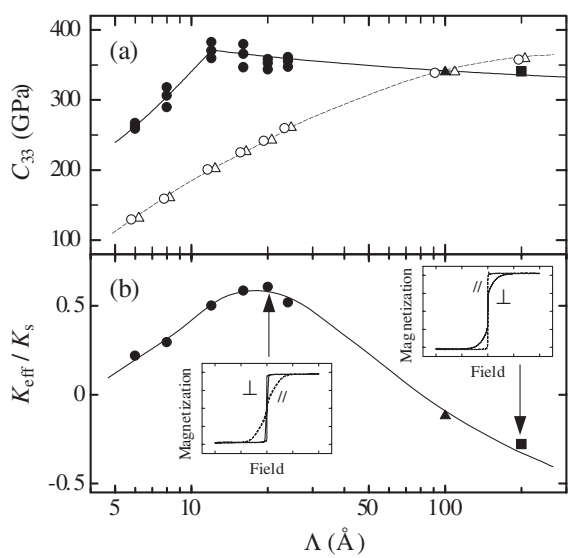

FIG. 2. Bilayer thickness dependence of C_{33} and $K_{\rm eff}$. (a) Solid marks denote the measured C_{33} of Co/Pt superlattice; circles, triangles, and squares indicate the Co-layer thickness of 4, 20, and 40 Å, respectively. Open circles and triangles denote the modulus calculated by the interfacial-strain-dependent model of Co(hcp)/Pt and Co(fcc)/Pt superlattice, respectively. (b) $K_{\rm eff}$ normalized by K_s. The insets show the typical magnetic hysteresis loops.

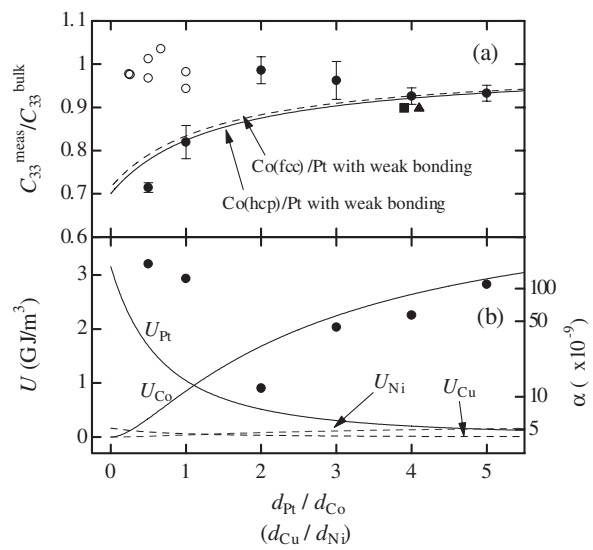

FIG. 3. Dependence of C_{33} and strain energy on the thickness ratio of Co/Pt and Cu/Ni superlattices. (a) Vertical axis is normalized by C_{33} of Co(hcp)/Pt or Cu/Ni superlattices. Solid and open symbols describe the measurements of Co/Pt and Cu/Ni superlattice, respectively. Solid and dashed lines are the normalized C_{33} of Co(hcp)/Pt and Co(fcc)/Pt superlattice calculated by the micromechanics theory, respectively. (b) Solid circles denote the degree of the volume fraction of the weak-bonding region α that gives the best fit to the measured C_{33} of Co/Pt superlattice. Solid lines denote strain energy in Co and Pt layers per unit volume of Co and Pt, respectively, and dashed lines are those of Cu and Ni layers per unit volume of Cu and Ni, respectively.

following equation assuming that the local C_{33} at the interfaces is lowered by the expansion of the interatomic distance.

$$\frac{C_{33}^{s}}{C_{33}^{0}} = \left\{1 - \frac{2m_i d_i}{\Lambda}\left(1 - \frac{2}{C_{33}^{i}}\frac{C_{33}^{\mathrm{Co}}C_{33}^{\mathrm{Pt}}}{C_{33}^{\mathrm{Co}} + C_{33}^{\mathrm{Pt}}}\right)\right\}^{-1}. \quad (1)$$

Where C_{33}^{0} is the macroscopic C_{33} without the interfacial softening. C_{33}^{Co} and C_{33}^{Pt} are those of bulk Co and Pt, respectively. m_i is the number of the layers where elastic softening occurs. d_i is the interatomic distance at the interfaces. C_{33}^{i} is the out-of-plane modulus at the interfaces, which is deduced by considering the adhesion between different metals as $C_{33}^{i}/C_{33}^{e} = 2/e^{a^*} - (1 + a^*)/e^{a^*}$ [22], where a^* is a scaled length defined by $a^* = (a - a_m)/l$. a, a_m, and l are the actual interatomic distance along the film-thickness direction, the average interatomic distance of Co and Pt, and a scaling length, respectively. C_{33}^{e} is the equilibrium interface elastic constant. a is measurable from the x-ray diffraction spectra [9], and l is given by Rose *et al.* [22]. According to this model, we calculated C_{33}, which is plotted in Fig. 2(a) by open marks. They are, however, much smaller than the measurements for $\Lambda = 6$–24 Å. Furthermore, PMA decreases when $\Lambda < 10$ Å indicating low lattice distortion, which would have caused a larger modulus if the interfacial-strain effect were dominant. Therefore, the interfacial-strain effect cannot be the dominant mechanism for C_{33}'s behavior.

Second is the intermetallic phase at the interfaces. There is a possibility of interdiffusion and formation of the CoPt intermetallic alloy at the interfaces [23]. Bandhu *et al.* [24] measured C_{ij} of Co_3Pt thin films, and they observed smaller C_{33} than that predicted from bulk C_{33} of Co and Pt: $C_{33}^{\mathrm{Co_3Pt}} = 308$ GPa, $C_{33}^{\mathrm{Pt(111)}} = 385$ GPa, $C_{33}^{\mathrm{fcc\text{-}Co(111)}} = 367$ GPa, and $C_{33}^{\mathrm{hcp\text{-}Co}} = 357$ GPa. This result implies that the existence of Co_3Pt interatomic alloy decreases the macroscopic C_{33} of Co/Pt superlattice. However, the rule of mixture predicted the decrease of the C_{33} by 15% for $\Lambda = 6$ and 8 Å at most even if all the Co layers were replaced into the alloy phase by the interdiffusion. Therefore, the Co_3Pt alloy cannot quantitatively explain the decreases of C_{33} at $\Lambda = 6$ and 8 Å. (Observed moduli were decreased by 20–30%.) Furthermore, considering that the alloy phase arises at the interfaces and its volume fraction is proportional to the number of the interfaces, alloy phase cannot explain the peak of C_{33} at $\Lambda = 12$ Å.

The third possibility is the formation of weak-bonding regions at the interfaces to relax the huge lattice-misfit strain. They decrease the macroscopic C_{ij}. We estimate this effect using the micromechanics theory considering that the Co/Pt superlattice is a multiphase composite consisting of Pt matrix and inclusions of Co and weak-bonding regions. We assume the Pt matrix to be isotropic for simplicity because an anisotropic matrix requires numerical calculations with many parameters for the Eshelby tensor [25]. This assumption is, however, acceptable, considering that we are interested in the relative change of the composite C_{33} for the Λ. Also, the elastic anisotropy factor of Pt is 1.6 and close to unity for an isotropic material, which supports this approximation. Co layers are assumed to be penny-shape inclusions, and the weak-bonding regions are replaced by the penny-shape microcracks. (Here, we neglect the effect of interfacial dislocations and delaminations on C_{ij}, because their effect is usually smaller than that of the microcrack while they release interfacial stress, and they are rather the origin of formation of the microcrack.) Minor axes of both inclusions are perpendicular to the film surface. We calculated the isotropic C_{ij} of Pt matrix using the Hill averaging method [26]. The rotation-symmetry axis of Co is set to be parallel to the minor axis of the penny-shape inclusions. The elastic constant matrix of the composite $\mathbf{C}_{\mathrm{Comp}}$ is then expressed by

$$\mathbf{C_{Comp}} = [f_m\mathbf{C_m} + f_{I_1}\mathbf{C_{I_1}}\mathbf{A_{I_1}} + f_{I_2}\mathbf{C_{I_2}}\mathbf{A_{I_2}}] \times [f_m\mathbf{I} + f_{\mathbf{I}_1}\mathbf{A_{I_1}} + f_{\mathbf{I}_2}\mathbf{A_{I_2}}]^{-1}. \quad (2)$$

Here, $\mathbf{I}$ is the unit matrix. Subscripts, m, I_1, and I_2 denote the matrix and inclusions, respectively. $\mathbf{C_i}$ and $\mathbf{A_i}$ are the elastic constant matrix and strain concentration factor of constitute i, respectively. According to the equivalent-inclusion theory [27] and the mean-field theory [28], $\mathbf{A_i}$ can be written as $\mathbf{A_i} = [\mathbf{S_i}\mathbf{C_m}^{-1}(\mathbf{C_i} - \mathbf{C_m}) + \mathbf{I}]^{-1}$ [25]. The Eshelby tensor $\mathbf{S}$ is given in terms of Poisson's ratio of the matrix and the aspect ratio of the inclusions.

The key parameters are the aspect ratios and volume fractions of the inclusions, which are closely related to each other. In order to approximate Co layers by penny-shape inclusions, the aspect ratio must be significantly small. Here we assume the aspect ratio to be 1.0×10^{-8} from the in-plane length of the specimen and Co-layer thickness. The aspect ratio of the microcrack is also assumed to be 1.0×10^{-8}. The volume fraction of Co is determined from the thickness ratio between Co and Pt layers. Although the volume fraction of the microcracks is uncertain, it should be proportional to the number of interfaces. Therefore, we assume it to be $\alpha \times f_{\mathrm{Co}}$. α is the proportionality constant and it is the only fitting parameter.

First, we assumed α to be independent of the thickness ratio, determined it by fitting the calculation to the measurement at $d_{\mathrm{Pt}}/d_{\mathrm{Co}} = 5$ (α was 1.1×10^{-7}), and compared the calculated C_{33} with the measurement in Fig. 3(a). As $d_{\mathrm{Pt}}/d_{\mathrm{Co}}$ decreases, C_{33} becomes smaller, because the volume fraction of the interface increases and the weak-bonding region increases. Calculated C_{33} shows good agreement with measured C_{33} at $d_{\mathrm{Pt}}/d_{\mathrm{Co}} = 0.5$, 1, 4, and 5, and we found that only the weak-bonding regions can explain the softening of the film at the small thickness ratio. However, we observe the discrepancies for $d_{\mathrm{Pt}}/d_{\mathrm{Co}} = 2$ and 3.

We investigate the origin of the difference at $d_{\mathrm{Pt}}/d_{\mathrm{Co}} =$ 2 and 3 by considering the relationship between the elastic

strain energy and α. The volume fraction of the weak-bonding regions must change depending on the thickness ratio. Therefore, we deduced α that gives the best fitting with the measured C_{33}, which are shown in Fig. 3(b) by solid circles. Then, assuming the complete bonding at the interfaces, we calculated the elastic strains of individual layers with the conventional continuum theory for the biaxial in-plane stress case. The strain energy per unit volume, U, is given by $U = \sigma\epsilon$, where σ and ϵ are the biaxial in-plane stress and strain, respectively. Figure 3(b) shows the result. As d_{Pt}/d_{Co} increases, U_{Co} increases and U_{Pt} decreases, and they intersect between $d_{Pt}/d_{Co} = 1$ and 2. Being close to this point, α takes a minimum. This result suggests that when d_{Pt}/d_{Co} is smaller, weak-bonding regions are induced to decrease U_{Pt}, and when it is larger, they are induced to decrease U_{Co}. At the same time, this result denies the conventional interpretation that the interfacial strain is the dominant factor for the lowered modulus in the superlattice systems. If it were the case, C_{33} should have shown a minimum around $d_{Pt}/d_{Co} \sim 2$, because when the volume fraction of the weak-bonding regions is the smallest, the strain at the interfaces becomes the largest. From these discussions, we attribute the lowered C_{33} to the weak-bonding regions between the Co and Pt layers. Considering that large strain caused by the lattice misfit is indispensable for PMA [14,15], negative K_{eff} indicates that when Λ is larger than 100 Å, Co/Pt superlattice barely grows epitaxially, and C_{33} can decrease at the interfaces. However, C_{33}/C_{33}^{bulk} at $\Lambda = 100$ and 200 Å is close to that at $\Lambda = 20$ Å because of the smaller volume fraction of the interface.

In order to confirm the validity of the above discussion, we further measured C_{33} of the Cu/Ni superlattice system. They were deposited on monocrystal Si substrates at the same condition as Co/Pt superlattice, and the thickness ratio of Cu to Ni d_{Cu}/d_{Ni} was ranged from 0.25 to 1 [d_{Cu}(Å)/d_{Ni}(Å) = 50/50, 10/10, 20/80, 4/16, 10/20, 5/10, and 10/15]. The number of bilayers was changed to keep the total film thickness of 800 Å for all specimens. C_{33} of Cu/Ni superlattice is plotted in Fig. 3, which are normalized by C_{33} predicted from the bulk materials' C_{33} [29,30]. Comparing to Co/Pt superlattice, significant softening was not observed even at the very small thickness ratio. Considering the elastic strain energy in Cu and Ni layers, this result is reasonable. In the Cu/Ni system, lattice mismatch at the interfaces is 2.6%, being smaller than that of the Co/Pt system, and C_{33} of Cu and Ni is smaller than those of Co and Pt. Therefore, elastic strain energy in Cu/Ni superlattice becomes smaller than that in Co/Pt superlattice [see the broken lines in Fig. 3(b)]. Thereby, the weak-bonding regions are barely induced at the interfaces, and the macroscopic C_{33} is comparable to the predictions.

Two important findings were observed in this study. One is the above-discussed strain-energy dependence of C_{33} of superlattice, and the other is the relationship between the elastic constants and PMA. Despite many studies, the origin of PMA has not been clarified yet, because of a number of possible factors and the ambiguity of bonding condition at the interfaces. However, the measurement of C_{33} enables one to predict the bonding condition through softening of C_{33}, which is a new approach for discussing the relationship between PMA and the interfacial bonding. Furthermore, it enables one to evaluate PMA nondestructively. Considering that picosecond-laser ultrasounds is a noncontacting technique, PMA can be evaluated during the deposition process in principle, and is applicable for industrial fields.

We are grateful to Dr. S. Morimoto, Osaka University, and Low Temperature Center, Osaka University, for the measurement of the magnetic properties.

*nobutomo@me.es.osaka-u.ac.jp

[1] W. M. C. Yang *et al.*, J. Appl. Phys. **48**, 876 (1977).
[2] M. R. Khan *et al.*, Phys. Rev. B **27**, 7186 (1983).
[3] B. M. Davis *et al.*, Phys. Rev. B **43**, 9304 (1991).
[4] K. Sakaue *et al.*, J. Magn. Magn. Mater. **126**, 207 (1993).
[5] H. Huang and F. Spaepen, Acta Mater. **48**, 3261 (2000).
[6] P. Villain *et al.*, Appl. Phys. Lett. **81**, 4365 (2002).
[7] I. K. Schuller and A. Rahman, Phys. Rev. Lett. **50**, 1377 (1983).
[8] D. Wolf and J. F. Lutsko, J. Appl. Phys. **66**, 1961 (1989).
[9] B. M. Clemens and G. L. Eesley, Phys. Rev. Lett. **61**, 2356 (1988).
[10] E. E. Fullerton *et al.*, J. Appl. Phys. **73**, 7370 (1993).
[11] H. Ogi *et al.*, Phys. Rev. Lett. **98**, 195503 (2007).
[12] S. Chikazumi, *Physics of Magnetizm* (Wiley, New York, 1964).
[13] P. F. Carcia *et al.*, Appl. Phys. Lett. **47**, 178 (1985).
[14] T. Kingetsu *et al.*, Sci. Tech. Adv. Mater. **2**, 331 (2001).
[15] Y. Kamada *et al.*, J. Appl. Phys. **90**, 5104 (2001).
[16] H. Kiessig, Ann. Phys. (Leipzig) **10**, 769 (1931).
[17] C. Thomsen *et al.*, Phys. Rev. B **34**, 4129 (1986).
[18] E. S. Fisher and D. Dever, Trans. Metall. Soc. AIME **239**, 48 (1967).
[19] R. E. Macfarlane *et al.*, Phys. Lett. **18**, 91 (1965).
[20] Z. G. Lin *et al.*, J. Appl. Phys. **73**, 2433 (1993).
[21] E. Lundgren *et al.*, Phys. Rev. B **62**, 2843 (2000).
[22] J. H. Rose *et al.*, Phys. Rev. B **28**, 1835 (1983).
[23] P. C. Mclntyre *et al.*, J. Appl. Phys. **81**, 637 (1997).
[24] R. S. Bandhu *et al.*, J. Appl. Phys. **91**, 2737 (2002).
[25] T. Mura, *Micromechanics of Defects in Solids* (Martinus Nijhoff, Dordrecht, 1987), 2nd ed.
[26] R. Hill, Proc. Phys. Soc. London Sect. A **65**, 349 (1952).
[27] J. D. Eshelby, Proc. R. Soc. A **241**, 376 (1957).
[28] T. Mori and K. Tanaka, Acta Metall. **21**, 571 (1973).
[29] H. Ogi *et al.*, J. Acoust. Soc. Am. **106**, 660 (1999).
[30] H. Ledbetter and S. Kim, in *Handbook of Elastic Properties of Solids, Liquids, and Gases* (Academic, New York, 2001), Vol. 2.